Surface & Coatings Technology 309 (2017) 641–650

Contents lists available at ScienceDirect

Surface & Coatings Technology

journal homepage: www.elsevier.com/locate/surfcoat

Microstructure and mechanical properties of cold sprayed 6061 Al in As-sprayed and heat treated condition

M.R. Rokni [a,*], C.A. Widener [b], O.C. Ozdemir [b], G.A. Crawford [b,*]

[a] M.C. Gill Composites Center, Department of Chemical Engineering and Materials Science, University of Southern California, Los Angeles, CA, USA
[b] Advanced Materials Processing Center, South Dakota School of Mines & Technology (SDSM&T), Rapid City, SD, USA

ARTICLE INFO

Article history:
Received 23 October 2016
Revised 6 December 2016
Accepted in revised form 9 December 2016
Available online 12 December 2016

Keywords:
Cold spray
Microtensile testing
Nanoindentation
Residual stress
Electron microscopy

ABSTRACT

Microstructural and mechanical properties of cold sprayed 6061 aluminum deposits on 6061-T6 aluminum alloy substrates are investigated under various heat treatment conditions, i.e. as-deposited, stress relieved and T6. The local mechanical property variation in the as-deposited material are explored using nanoindentation technique, and correlated with microstructural characterization conducted via electron back-scattered diffraction. It is found that the prior particle boundaries have ~0.4 GPa higher hardness than particle interiors, which is attributed to grain refinement in these regions promoted by local dynamic recrystallization. Also, the bulk-scale mechanical properties of the deposits are evaluated by microtensile testing in various post-heat treatment conditions and compared to those of conventionally processed 6061-T6 aluminum. The as-deposited material showed markedly higher ultimate strength (~460 MPa) and lower ductility (~3%) compared to conventionally processed material and this is attributed to significant cold working during the cold spray deposition process and associated grain boundary strengthening and dislocation strengthening mechanisms. Heat treated specimens showed a slight improvement in both ultimate strength and ductility compared to the as-deposited condition. These improvements are attributed to an improvement in metallurgical bonding at prior particle boundaries and a modest increase in the density of strengthening precipitates. Fractography of the specimens revealed that the heat treatment also changes the fracture characteristics of the cold sprayed 6061 aluminum deposit. The residual stress profiles and bond strength of the deposits are also studied using x-ray diffraction, tensile pull-off and three lug shear testing, respectively.

1. Introduction

Cold Spray (CS) processing is a solid state materials deposition process which depends on severe plastic deformation (SPD) of process powder to achieve a dense deposit [1–4]. CS systems can be categorized into two types, i.e. low-pressure and high-pressure cold spray (HPCS), where the latter has become increasingly common because of a higher processing gas pressure and temperature. Consequently, HPCS enables the fabrication of dense deposits with reduced interparticle voids and porosity, leading to improved properties/performance (e.g. mechanical [5–7], electrical [8,9], and wear [10,11]).

During HPCS, plastic strains can reach ~10 (corresponding to strain rates of 10^6/s to 10^9/s) in some regions of the deposition [3,5,12,13], however, other regions, particularly particle interiors, experience much less strain, and the final microstructure is heterogeneous as a consequence of the non-uniform deformation [5,12–19]. As such, it is important to evaluate the effect of non-uniform deformation on the microstructure and micro-scale mechanical property variation throughout the CS deposit.

HPCS processing has gained increasing interest for its use in repair and refurbishment of damaged metallic components, particularly in defense and aerospace industries. CS deposits, however, typically exhibit poor ductility and high hardness as a consequence of a heavily cold worked microstructure, that may contain some degree of porosity and interparticle voids [5–9]. Thus, the bulk-scale mechanical properties (e.g. tensile strength and elongation to failure) of CS processed deposits need to be investigated, as repaired components are expected to perform at the same level as undamaged, conventionally processed components. To this end, systematic study, to the authors' knowledge, of strength, elongation and fracture behavior of CS depositions using microtensile testing has yet to be reported.

Moreover, post-deposition heat treatment is often employed to improve mechanical performance of CS deposits [6,9,20–22]. In precipitation hardenable alloys, however, such as Al 6061 (the subject of this study), it is important to consider the influence of heat treatment on precipitation strengthening. SPD processes often result in varied precipitation behavior and associated strengthening effect when compared to conventionally processed material [23–28]. Thus, designing

* Corresponding authors.
E-mail addresses: rokni@usc.edu, mreza.rokni@gmail.com (M.R. Rokni), grant.crawford@sdsmt.edu (G.A. Crawford).

http://dx.doi.org/10.1016/j.surfcoat.2016.12.035
0257-8972/

and optimizing a single heat treatment for CS deposits of the same material class (e.g. Al alloys), may not be possible, and evaluating conventional heat treatments provides a useful starting point.

As with all thermal spray processes, the presence of residual stress in the coating and near the coating/substrate interface can influence the mechanical performance of CS deposits [29–31]. In the case of HPCS, SPD generates residual stress in the CS deposit, and microscopic interpretation of the residual stress profile (i.e. on the scale of a particle) is not straightforward and requires knowledge of many details of the deposition process, such as non-uniform local deformation and recrystallization. As a result, investigating the effect of CS processing on the residual stress distribution in the deposits, while also considering related micro- and macro-scale mechanical properties, is of the interest in the present study.

With continued interest in using HPCS for repair applications, there is an increasing need for systematic studies which evaluate the processing, microstructure, and mechanical behavior of relevant defense and aerospace alloys, processed via CS. 6061 Al is one such alloy [8,17,32] and is the subject of this study. This paper presents the effect of HPCS and post-CS heat treatment on microstructure and mechanical properties of CS 6061 Al. Local mechanical property variation was probed using nanoindentation and correlated with microstructural analysis conducted via electron backscattered diffraction (EBSD). Also, bulk-scale mechanical properties of the deposit were evaluated by microtensile testing. The effect of stress relief and T6 heat treatments on microstructure and mechanical properties of the CS 6061 deposition was also investigated. The residual stress profiles and bond strength of the deposits were also explored using x-ray diffraction (XRD), and tensile pull-off and three lug shear testing, respectively.

2. Experimental procedure

2.1. Cold spray processing

Gas-atomized 6061 Al powder (Valimet, CA, USA) with an average size of 38.7 ± 17.3 μm was deposited on 6061-T6 Al substrates, which were grit blasted prior to coating deposition. The size distribution of powder particles was measured using a laser diffraction particle analyzer (S3000, Microtrac, Montgomeryville, PA). Cold spray deposition was performed using a high-pressure CGT 4000 cold spray system (CGT Technologies, Munich, Germany) and helium carrier gas. The helium gas pressure and temperature, near the heater exit, were maintained at 2.8 MPa and 400 °C, respectively. For these experiments, helium gas was chosen over nitrogen because it results in a much higher sonic velocity, due to a lower molecular weight and higher specific heat ratio. The deposit was made to a total thickness of 10 mm.

2.2. Design of microtensile samples

Uniaxial tensile testing was carried out at room temperature with a loading rate of 200 μm/min in a universal testing machine (MTS 810, MTS Systems Corporation, Minneapolis, MN, USA). Tensile testing coupons were machined from the as-deposited cold spray samples with the dimensions shown in Fig. 1. These specimens were fine polished on both sides to remove surface discontinuities, resulting in a final thickness of 1.0 mm. Specimens were machined such that the tensile loading axis was oriented perpendicular to the spraying direction. A total of 12 samples were tested including three samples for each of the following conditions, as-deposited, stress relieved, T6 aged, and substrate material (bulk).

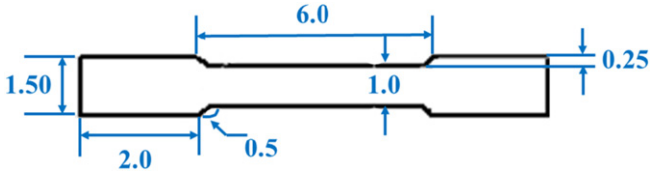

Fig. 1. Specimen geometry used for microtensile testing. All dimensions are in mm.

2.3. Heat treatments

To evaluate the influence of heat treatment on the as-deposited cold spray microstructure three conditions were evaluated: as-deposited (AD, no heat treatment), stress relieved (SR), and T6 condition. Furthermore, the 6061 Al substrate material was received from the manufacturer in T6 condition. Stress relief and T6 conditions were chosen as they are common commercial heat treatments for 6061 Al alloy. All heat treatments were performed in an open air furnace (Lindburg 51894, Riverside, MI). Table 1 summarizes the heat treatment procedures used in this study.

2.4. Microstructure characterization

The microstructure of the as-received powder and CS deposits in different conditions were characterized using TEM, SEM, and EBSD. TEM micrographs were obtained using a JEM-2100 LaB_6 (JEOL Ltd., Tokyo, Japan) operated at 200 kV. Thin discs, 3 mm in diameter, were excised from the deposition, and then polished, dimpled, and ion milled for 4 h. SEM and EBSD analyses of the as-received powders and cold spray depositions were conducted using a field emission SEM (Supra-40, Zeiss, Oberkochen, Germany) operated at 15 kV. EBSD samples were sectioned from the CS deposition and prepared by standard metallographic techniques. Final polish was conducted using a 0.05 μm diameter colloidal silica suspension and vibratory polishing.

2.5. Micro- and nanohardness testing

Nanoindentation tests were conducted using a commercial nanoindenter (MTS Nanoindenter XP; Keysight Technologies, Santa Rosa, CA) in load control with a maximum load of 10 mN while using a Berkovich indenter. A square array of 121 indents with 10 μm intervals were made to obtain hardness measurements from various regions of the deposition, e.g. prior particle boundaries (PPBs) and particle interiors. The Oliver and Pharr method [34] was used to determine hardness and the elastic modulus of the corresponding deposition. No significant variation of elastic modulus was observed throughout the deposit. Thus, the modulus data was omitted from this report.

Vicker's microhardness measurements were also performed on the CS 6061 Al layer in as-deposited and heat treated conditions as well as the bulk 6061-T6 material using a Vicker's microhardness tester (HMV-2, Shimadzu, Tokyo, Japan) under an indenter load of 300 g. Ten microhardness measurements were collected and reported along with the standard deviations for all four conditions.

2.5.1. Residual stress measurement

The internal residual stresses of the cold sprayed aluminum sample were characterized using an X-ray stress analyzer (LXRD®, Proto, Canada). A ceramic X-ray tube with a chromium target was used for x-ray generation. Standard samples were evaluated prior to each test to confirm the XRD system was in working condition. All tests were performed using a large aperture (2 mm × 5 mm) to maximize the signal strength. The cold spray specimen was electrochemically polished to

Table 1
Heat treatment conditions for SR and T6 treatments [33].

Heat treatment	Temperature (°C)	Time
SR	176	1 h
T6	176	8 h

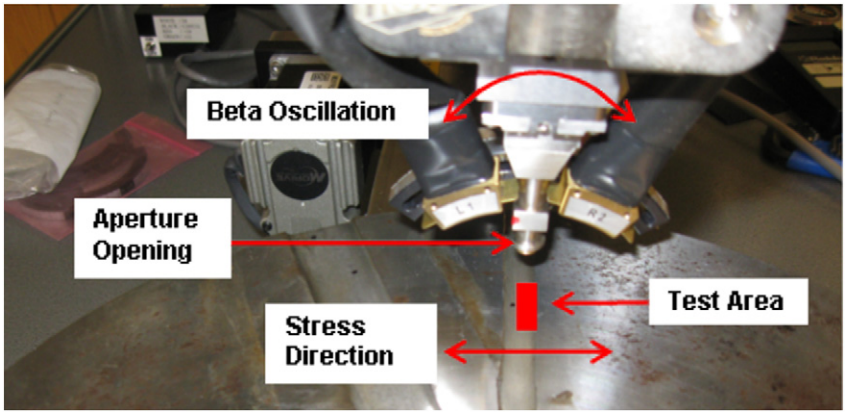

Fig. 2. Residual stress experimental setup.

relieve the surface stresses introduced by cutting the sample. The goniometer was focused at multiple locations on the specimen cross-section and oscillated at a specified beta angle to obtain residual stress profiles in both the x- and z-directions. Fig. 2 shows the residual stress measurement configuration while Fig. 3 shows measurement locations, in both the x- and z-directions, on the specimen surface. The red dashed arrow in Fig. 3 shows the direction of sampling from the 0 mm reference location. This test region was selected to capture the residual stress profile from the substrate into the deposit. 14 measurement locations were tested in the z-direction, and 11 locations were tested in the x-direction.

2.5.2. Adhesion and shear strength

The adhesion strength of the cold spray deposit to the underlying substrate was evaluated using a standard tensile pull-off method (ASTM C633). Per the specification, the deposit was ground to an 8 mm thickness to create a uniform surface. The coated surface was then bonded to a bare slug using a high-performance epoxy adhesive (FM1000, Cytec Industries, Woodland Park, NJ). The coupon dimensions used for adhesion testing had a 25 mm diameter. Adhesion testing was carried out using a servo-hydraulic uniaxial testing system (MTS 810, Systems Corporation, Eden Prairie, MN) in displacement control with a crosshead speed of 10 mm/min. Maximum load at failure was recorded and the maximum tensile stress was reported as the adhesion strength of the deposit. Failed samples were visually inspected to determine the mode of failure. The primary failure modes of interest in this system include; (1) adhesive failure at deposit/substrate interface, (2) cohesive failure of the deposit, and (3) cohesive failure of the glue. Three samples were tested and the average adhesion strength was reported.

To study the adhesive shear behavior of the CS 6061 deposition, a three lug shear test (MIL-J-24445A [35]) was performed. Specimens were tested in a universal tensile testing machine (MTS 810, Systems Corporation, Eden Prairie, MN) under displacement control at constant cross-head speed of 1 mm/min. The applied load was measured continuously with a 25 kN load cell. The force required to shear the deposit was used to determine the shear strength of the bond. The adhesive shear testing arrangement is shown in Fig. 4. As shown in this figure, three lugs were tested and the average shear strength was reported.

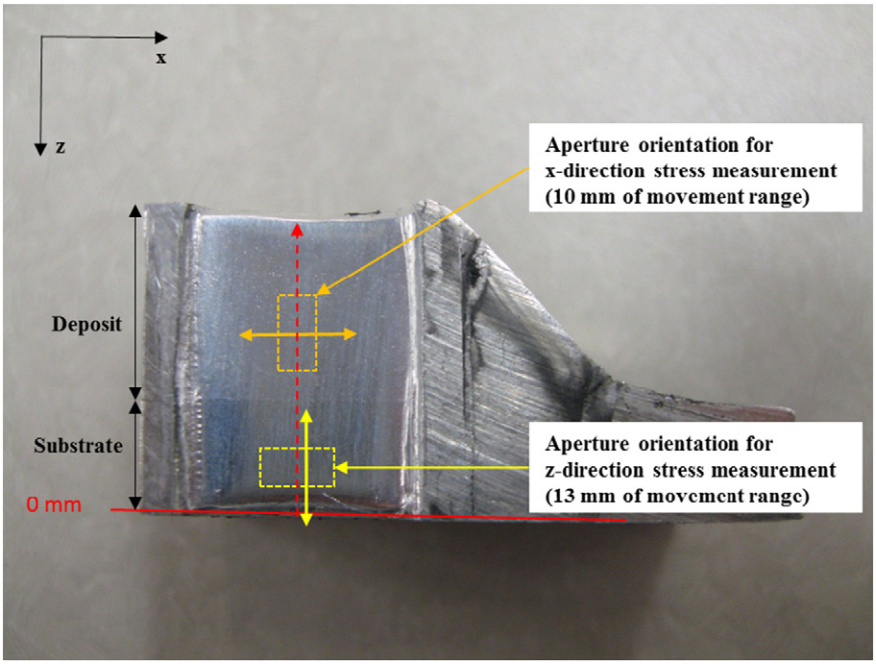

Fig. 3. Residual stress measurement orientations.

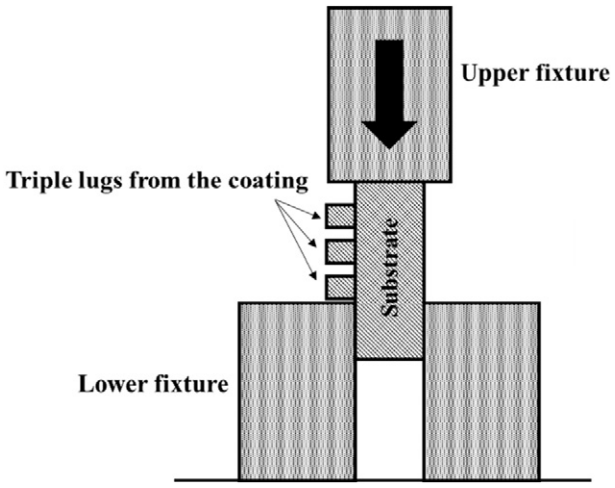

Fig. 4. Schematic of the shear test fixture (after [26]).

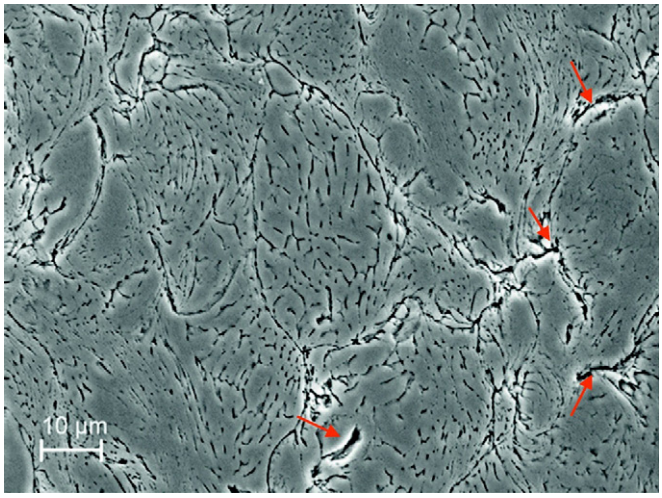

Fig. 6. SEM cross-sectional micrograph from the CS 6061 deposit showing the particle morphologies after CS and the presence of interparticle voids and porosity (red arrows).

3. Results and discussion

3.1. Microstructural characterization

3.1.1. As-received powder

Fig. 5 shows SEM images obtained from the feedstock 6061 Al powder. In general, powder particles were characterized by a spherical morphology with some particles showing a rounded morphology. Laser particle analysis revealed an average particle size of 38.7 ± 17.3 μm. Fig. 5(b) shows the surface grain structure of the as-received powder particles and demonstrates the powders are characterized by 1–4 μm surface grain size. According to a previously published study by the authors [16,17], a similar grain structure is typically also present inside the powder particles with some solute segregation at the grain boundaries.

3.1.2. Cold sprayed deposition

Fig. 6 shows a cross-sectional SEM image of the CS 6061 Al deposition parallel to the spraying direction. From inspection of Fig. 6, the deposition shows some evidence of interparticle voids and porosity indicated by red arrows. These voids generally form due to the lack of local deformation in some particles caused by lower particle impact velocity [7,13,18]. The influence of these imperfections on the mechanical behavior of the deposit will be discussed later in this paper.

EBSD mapping (Fig. 7) was performed to characterize the grain structure in different regions of the CS deposit. The analysis revealed the presence of two distinct regions within the CS deposit. First, particle interiors were characterized by a 1–10 μm grain size and a moderate density of low angle grain boundaries (LAGBs). The latter is attributed to significant plastic deformation experienced by the powder particles during the CS deposition process. Second, prior particle boundary (PPB) regions are characterized by much smaller grain size including both pancaked and ultra-fine grain (UFG) structures. The presence of UFG structures in CS deposits has been well documented and is often attributed to both continuous (CDRX) and geometric dynamic recrystallization (GDRX) phenomena [12,14,17,36–38] which occurs because of the high degree of plastic deformation (strain rates of 10^6/s to 10^9/s) and moderate temperatures (>200 °C) experienced at PPBs during the deposition process.

3.2. Nanohardness

Nanoindentation was performed on the as-deposited CS deposit to evaluate the local mechanical property variation within the microstructure. Fig. 8 shows an optical micrograph of a square nanoindentation array (121 indentations) in the CS 6061 deposit. From inspection of Fig. 8, the testing area is generally free of voids or porosity. This is an important observation for these studies as the presence of porosity and voids can affect the size and depth of indentations during low load nanoindentation studies [2,5].

Fig. 9(a) presents a nanohardness contour map of the 150 μm × 150 μm test region. The map clearly shows a non-uniform hardness distribution in the CS 6061 deposit. Comparison of Figs. 8 and 9(a) indicates that the higher hardness regions are generally associated with PPBs whereas, the lower hardness regions are typically found in particle interiors. As such, each indentation was carefully inspected to assess if

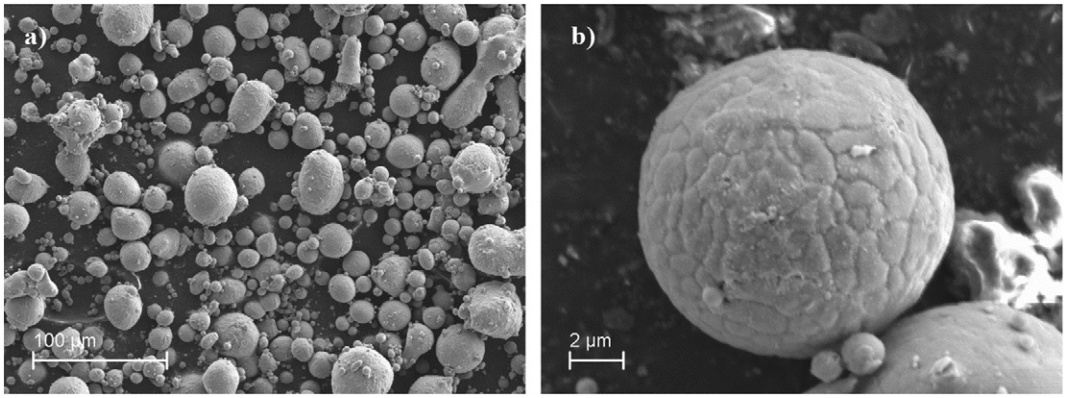

Fig. 5. SEM micrographs of the as-received 6061 Al powder showing a) powder morphology, and b) surface grain structure.

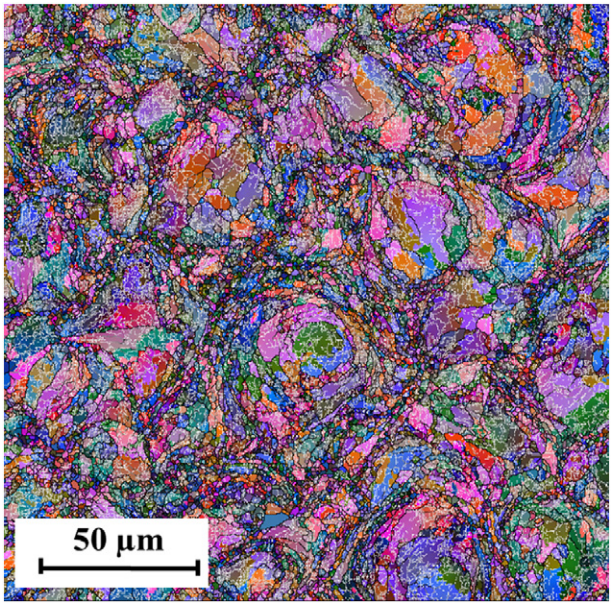

Fig. 7. EBSD map from the CS 6061 deposit showing the grain size difference between PPBs and particle interiors.

the indentation was located in a particle interior or near a PPB region. Fig. 9(b) provides a comparison of the nanohardness between these two regions in the CS deposit. Clearly, the hardness values for PPBs (1.77 ± 0.13 GPa) is higher than those of the particle interiors (1.43 ± 0.15 GPa), as listed in Table 2. This is indeed consistent previously published findings on CS deposition of both pure metals (Ni [12], Cu [12], and Ti [19]) and alloys (7075 Al [5] and 5083 Al [13]). Moreover, higher hardness near PPBs can be attributed to grain boundary strengthening that results due to the fine grain size in these regions.

It is important to note, although particle interiors have lower hardness than PPBs the hardness in these regions (particle interiors) is significantly higher (see Table 2) than that of the feedstock powder (0.98 ± 0.12 GPa). The increase in the hardness of the particle interiors following CS deposition can be attributed to the strain hardening effects, and associated increase in dislocation and LAGB density (white lines in Fig. 7), experienced as a result of the deposition process. Once again, these findings are consistent with those reported for other material systems [5,12,13,18,19,36].

3.3. Residual stress profiles

The x- and z-direction residual stress profiles determined by XRD are plotted in Fig. 10. To avoid edge effects at the free surfaces, readings obtained from the bottom of the substrate and the top of the deposit were disregarded. The z-direction profile in Fig. 10 shows significant compressive residual stress (~30–90 MPa) in the substrate near the deposition interface. This is attributed to (i) a sudden halt of the carrier gas at the surface of the substrate and associated rise in gas temperature, and (ii) peening effect of impacting particles at the substrate surface. Thus, elevated temperatures, particle impact, and gas exertion on the substrate surface result in compressive residual stress in the substrate in the deposition direction. However, this compressive stress is balanced by a tensile stress in the x-direction due to the shape of the substrate (flat plate).

The deposit is characterized by a compressive residual stress in the z-direction near the substrate interface, gradually dissipating toward the top of the deposit. This occurs due to severe deformation of powder particles on the cold substrate surface and is compounded by the shot peening effect [39–41] of subsequently arriving particles/layers. With increasing deposition thickness the shot peening effect gradually reduces and the deposition temperature increases resulting in reduced compressive stress. In addition, as can be seen in Fig. 10, the compressive residual stress in the z-direction is, once again, balanced by a tensile

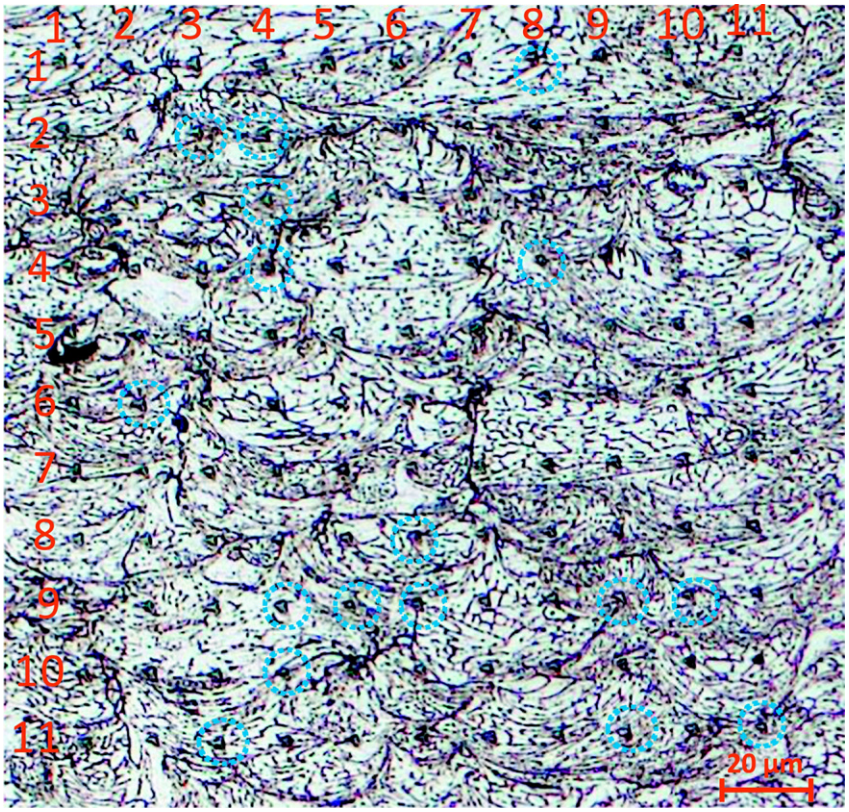

Fig. 8. Optical micrograph showing a square array of nanoindentations on the CS 6061 Al deposit.

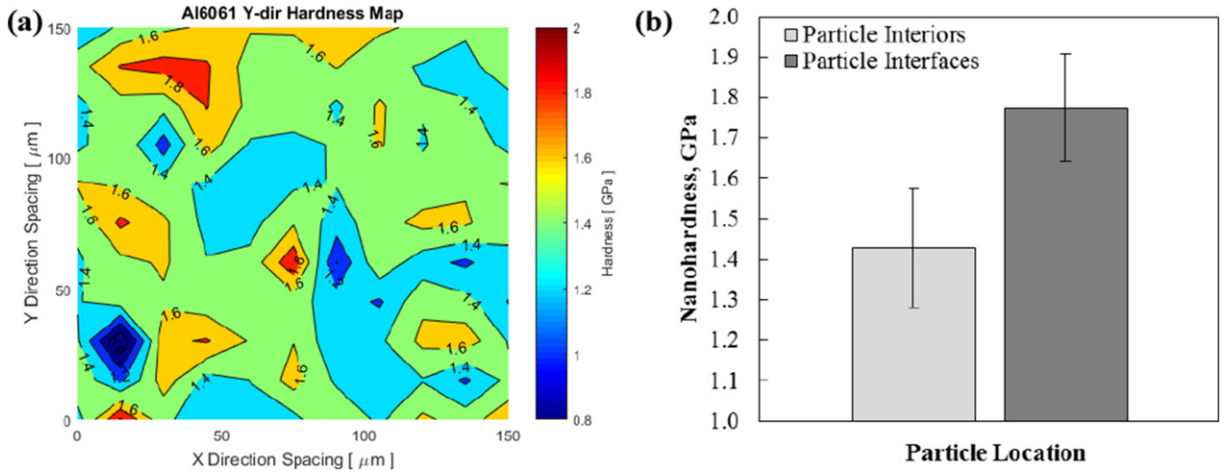

Fig. 9. (a) Counter map showing the local nanohardness distribution, and (b) nanohardness obtained from particle interior and PPB regions of CS 6061 deposit. Error bars represent one standard deviation.

stress in the x-direction near the substrate/deposit interface and is associated with particle flattening during impact.

3.4. Post-CS heat treatment

CS deposits often suffer from reduced ductility compared to conventionally processed bulk material [1,3,5,6]. Post-CS heat treatment is considered a viable method for improving ductility of as-deposited material [6,20–22]. This section reports on the effect of post-CS heat treatment on the microstructure and mechanical behavior of 6061 Al deposit fabricated by CS. In this regard, two 6061 Al commercial heat treatments were used, i.e. stress relief annealing (SR) and peak aging (T6). These results were then compared to the as-deposited (AD) condition.

3.4.1. Microstructural characterization

Fig. 11 shows TEM micrographs of CS 6061 Al deposits in AD, SR, and T6 condition. Recall, the AD microstructure was characterized by a moderate dislocation density (Fig. 11(a)) and multiple LAGBs (Fig. 7). As shown in Fig. 11(b), the SR sample is characterized by the presence of multiple well-defined ultrafine grains with moderate dislocation density within grains. Comparing the AD and SR microstructures it is evident that some recovery has occurred after stress relief annealing. In T6 condition, the microstructure (Fig. 11(c)) is characterized, once again, by the presence of UFG structures but also by a significant reduction in dislocation density, indicating that significant recovery has occurred in the microstructure during the aging process. The microstructure in T6 condition was characterized by the presence of some GP zones and β' phase (Mg_2Si) precipitates having diameters ranging from ~20 to 200 nm. As shown by red arrows in Fig. 11, precipitation in this condition tends to be localized at pre-existing GBs. Because some grains did not fully recover during heat treatment, interior dislocations act as inhomogeneous nucleation sites for precipitation, which resulted in very fine distribution of precipitates in some grain interiors, shown by red-dashed ellipse in this micrograph.

Based on our analysis, including multiple TEM micrographs in this material, the precipitate morphology in the T6 condition differs from what is commonly reported for 6061 Al alloy, where spherical (or needle-shaped) GP zones (~5 nm), needle-shaped β'', rod-shaped β', and disc-shaped β particles have been reported. Moreover, the overall precipitate density in the T6 treated CS material is low compared to that typically reported for 6061 Al in T6 condition. This observation likely indicates a variation in precipitation behavior caused by the presence of a heavily deformed microstructure in the as-deposited material. A similar phenomenon has been reported by Kim et al. [23] and Rezaei et al. [24] for equal-channel angular pressing (ECAP) and accumulative roll bonding (ARB) processed 6061 Al alloy.

Table 2
Nanohardness obtained from the feedstock 6061 Al powder and CS deposit. Results include average ± standard deviation.

Material	6061 powder	CS 6061 deposit	
		Particle interior	Prior particle boundaries
Hardness (GPa)	0.98 ± 0.12	1.43 ± 0.15	1.77 ± 0.13

3.4.2. Tensile properties and microhardness

Fig. 12 shows characteristic engineering stress-strain curves for the 6061 Al substrate and CS samples in AD, SR, and T6 condition. Ultimate tensile strength (UTS) and percent elongation were extracted from the stress-strain curves, for each sample, and are summarized in Fig. 13. Furthermore, as seen in the figure, the values for the bulk 6061-T6 are reported on the top left corner on the graphs.

Fig. 13(a) shows that cold spray processing results in a remarkable 52–70% (depending on treatment, i.e. AD, SR, T6) improvement in UTS as compared to bulk 6061-T6 material. This increase in strength is attributed to severe plastic deformation experienced by the material during CS and is primarily driven by grain refinement and strain hardening mechanisms [1,3,5,12]. Similar trends have been reported for 6061 Al alloy processed by other severe plastic deformation processes such as, ARB (46% increase) [24], ECAP (60% increase) [25], high pressure torsion (92% increase) [26], cryogenic rolling (46% increase) [27], and tube channel pressing (39% increase) [28].

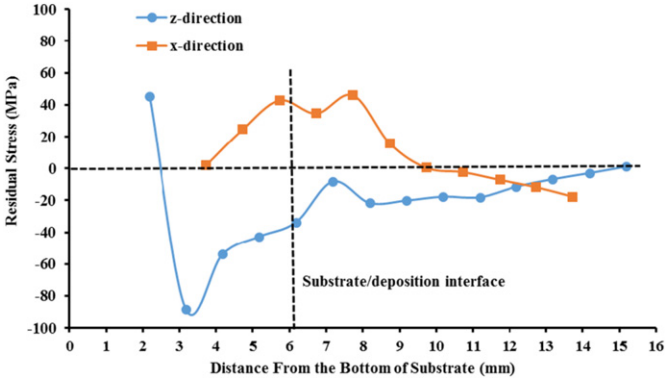

Fig. 10. Normal (z-direction) and transverse (x-direction) residual stress profiles obtained as a function of depth within the substrate and deposit.

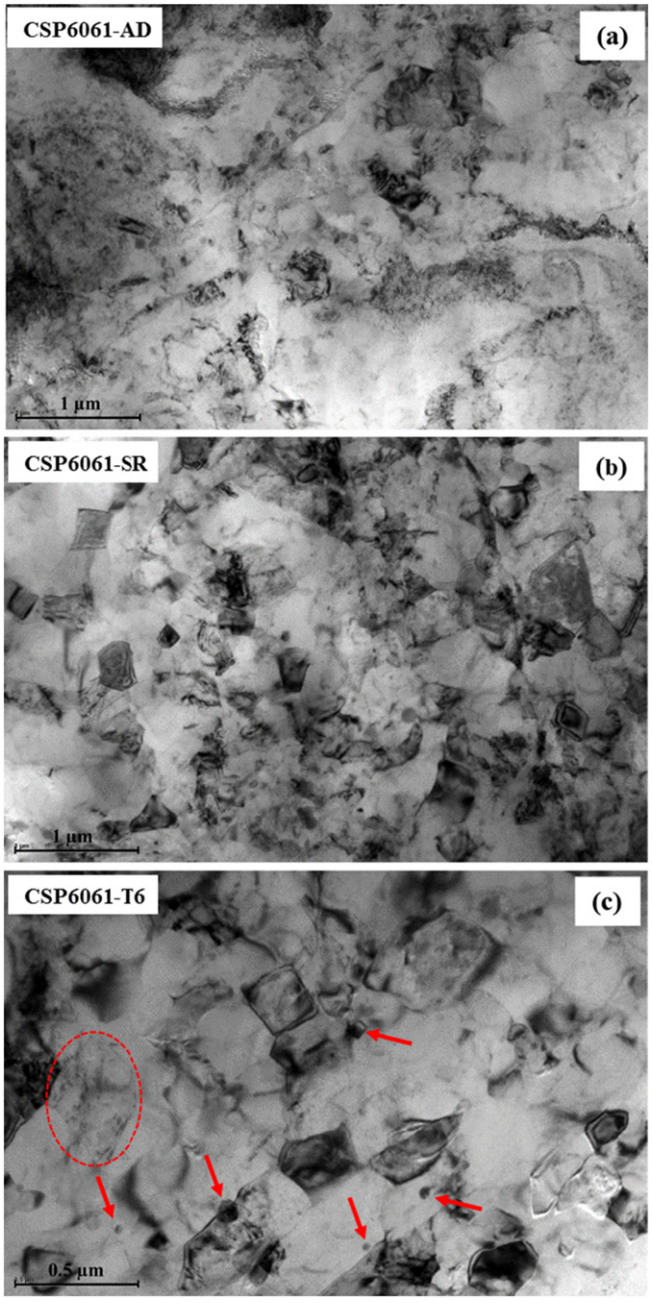

Fig. 11. TEM micrographs of the CSP 6061 deposition in (a) as-deposited (AD) condition showing moderate dislocation density and multiple LAGBs, (b) stress relieved (SR) condition showing well-defined ultrafine grains with moderate dislocation density within grains, and T6 conditions showing significant reduction in dislocation density in UFG structure. Red arrows indicate the presence of precipitates on pre-existing GBs.

Also, from inspection of Fig. 13 the UTS did not increase significantly after post-CS heat treatment (UTS for AD samples was only slightly lower than SR or T6 samples). While the increase in UTS for SR and T6 samples can largely be attributed to the formation of strengthening precipitates (i.e. GP zones and β), the increase in UTS is relatively small. This provides an indication that the as-deposited microstructure, consisting of UFG structures in PPB regions, moderate dislocation density in particle interiors, and GB segregation has a significant influence on precipitation phenomena. The same behavior has been reported for precipitation strengthened alloys subjected to other severe plastic deformation processes [42–44]. Schoenung et al. [42] investigated strengthening

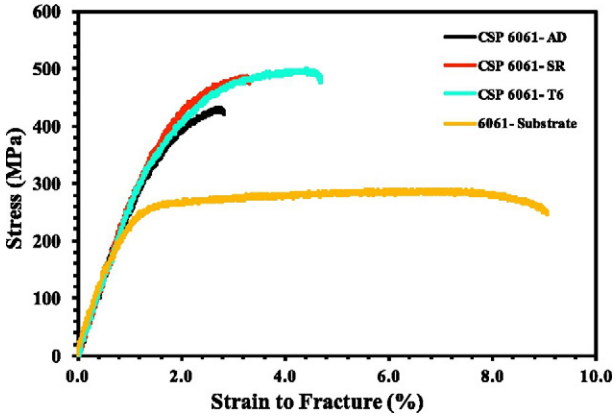

Fig. 12. Microtensile stress-strain curves for 6061 Al substrate and CS deposition in AD, SR, and T6 condition.

mechanisms of 7075 Al alloy fabricated through cryomilling, degassing, hot isostatic pressing and extrusion, followed by a subsequent heat treatment. Investigators reported that both natural and artificial (T6 treatment) aging in the 7075 Al alloys with UFG structures resulted in limited increase in strength. Thus, it seems rational to have relatively small increments in UTS values after heat treatment in the present study.

Furthermore, while CS resulted in an increase in UTS compared to the conventionally processed substrate material, the process also

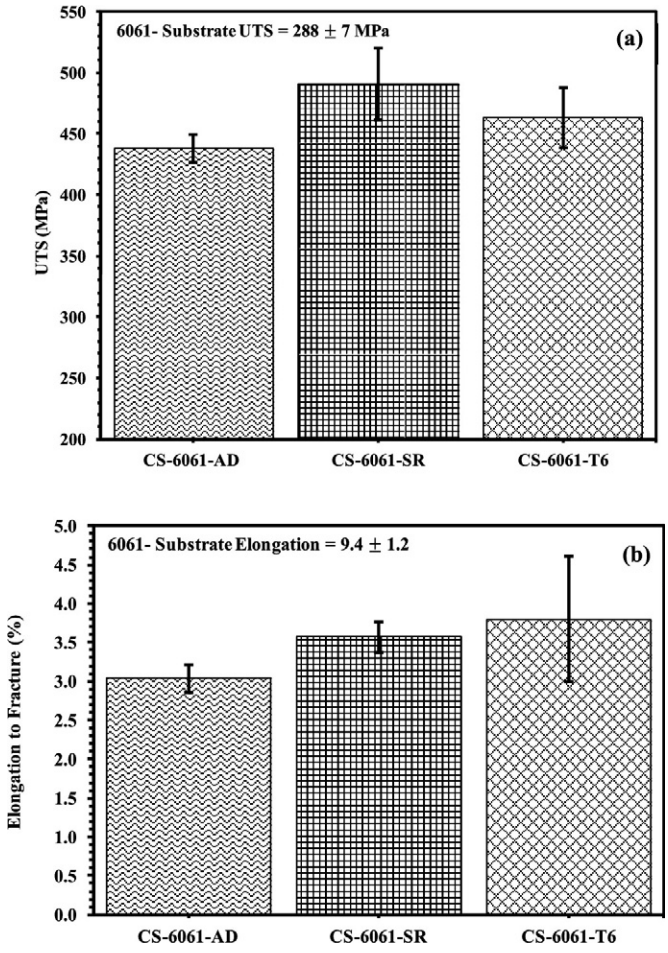

Fig. 13. The (a) UTS and (b) elongation to fracture of microtensile specimens of the CS 6061 Al deposit in AD, SR, and T6 condition. Values for the bulk 6061-T6 substrate are shown on the top left corner for comparison.

resulted in a marked reduction in ductility, as shown in Fig. 13(b). This decrease in ductility is attributed to the significant cold working during CS as well as the presence of some interparticle voids and porosity (Fig. 6), as discussed in Section 3.1.2. On the other hand, Fig. 13(b) shows that post-CS processing did improve ductility to some degree. This could be related to the occurrence of some increase in metallurgical bonding due to localized improvement in metallurgical bonding at the PPBs during heat treatment [8,9,21,22,45–47].

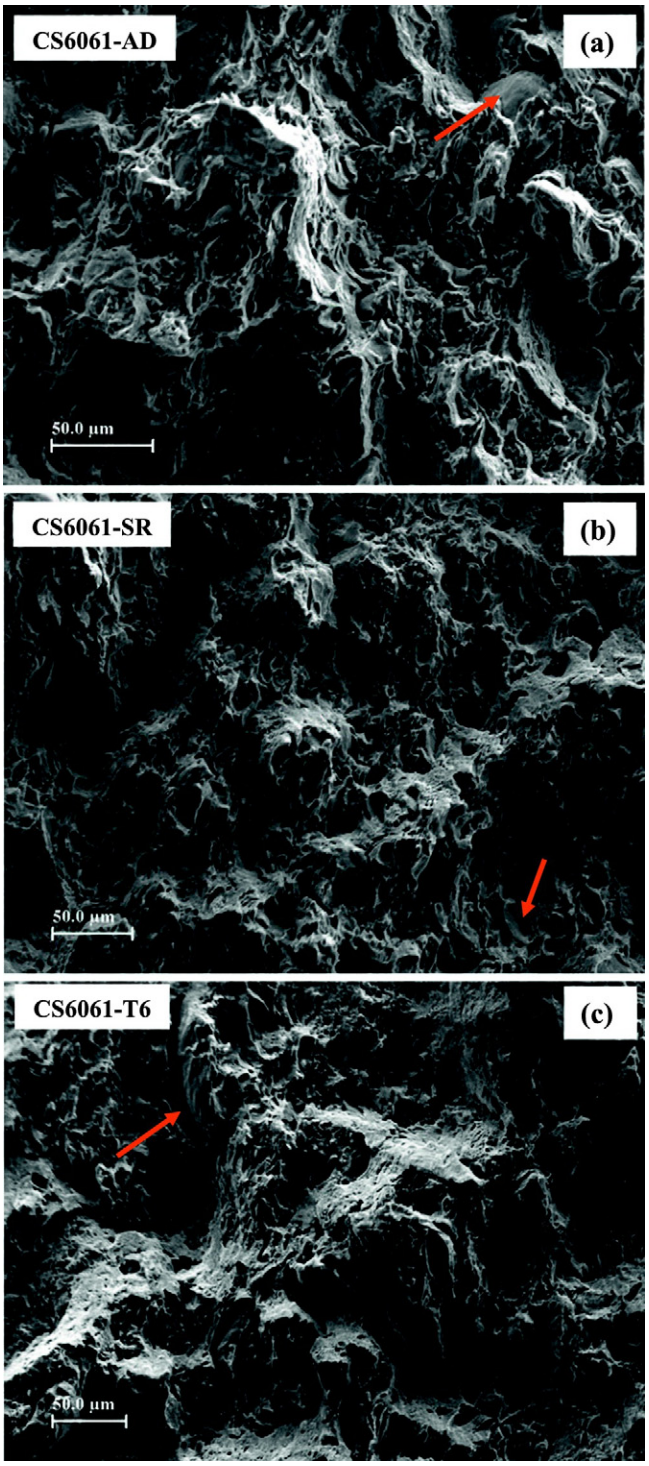

Fig. 14. SEM micrographs showing the fracture surface of microtensile specimens of the CS 6061 deposit in (a) as-deposited (AD), (b) stress relieved (SR), and (c) T6 conditions. Red arrows highlight smooth fracture regions indicative of particle-particle decohesion.

3.4.3. Fractography

To obtain detailed information on the deformation mechanisms of the as-deposited and heat treated deposits, fracture surfaces of the microtensile samples were analyzed and are presented in Fig. 14. Fracture surface morphologies in AD, SR and T6 conditions are characterized by two primary features (1) ductile micro-void coalescence and tearing ridges, and (2) smooth regions indicative of particle-particle fracture. The latter leads to brittle behavior (low strain to failure) and rapid crack propagation, which could explain the limited ductility of CS 6061 Al. The cracks predominantly initiated at the PPBs and propagated along the interfaces rather than through the deformed particles, as indicated by red arrows in Fig. 14. Based on fractographic analysis there appears to be a general decrease (although slight) in particle-particle fracture regions in the heat treated specimens as compared to the AD material.

3.4.4. Bond strength

To probe the quality (cohesive/shear strength) of the cold spray deposition and the adhesion of the deposit to the underlying substrate, adhesion testing was performed. Table 3 shows the results of both tensile and shear adhesion testing of the 6061 Al CS deposition. For all cases, cohesive failure was observed within the CS deposition (as opposed to adhesive failure at the substrate/deposit interface). As such, we can infer that the tensile adhesive bond strength must exceed the average cohesive strength determined using tensile pull-off testing, i.e. 78.2 ± 2.3 MPa. This value is higher than that generally reported in the literature for CS Al depositions (40–70 MPa) [48–52], an indication of the quality of the CS depositions in this study. Clearly, the adhesion strength at the substrate/deposit interface is good, resulting in a cohesive failure. Furthermore, the residual stress distribution within the CS deposition likely encourages cohesive failure. Here, compressive stresses (z-direction) near the substrate interface (Fig. 10) counteract the tensile stresses imposed during adhesion testing. With increasing distance from the substrate interface (increased deposition thickness) the compressive residual stress dissipates and the applied tensile stress increases, encouraging cohesive failure away from the substrate interface. Shear adhesion testing, performed by three-lug shear method, yielded shear strengths of 72.5 ± 3.1 MPa within the deposition. Once again, failure occurred within the CS deposition, indicating the shear adhesion strength exceeds this value. As expected (considering the testing geometry), tensile adhesion strengths exceeded shear values. Regardless, these results indicate that the deposition reported here is of good quality and has excellent adhesion strength.

4. Summary

This study investigated the microstructure and mechanical properties of 6061 aluminum deposits fabricated by HPCS. Local mechanical property variation was investigated using nanoindentation in conjunction with EBSD and results showed the presence of UFG structures located near PPBs gave rise to a ~ 0.4 GPa increase in nanohardness compared with particle interiors. X-ray diffraction measurements revealed a state of compressive residual stress both in the deposit and the substrate in

Table 3
Summary of tensile and shear adhesion strength results for 6061 Al cold spray deposits on a 6061 Al substrate obtained by tensile pull-off and three lug shear testing. Results include average ± standard deviation.

Tensile adhesion strength (MPa)	Shear adhesion strength (MPa)	Mode of failure
78.2 ± 2.3	72.5 ± 3.1	Cohesive

the direction of CS and tensile residual stress in the transverse direction near the substrate/deposition interface. Microtensile testing showed that while CS processing leads to a marked increase in UTS, it causes a significant decrease in ductility of the 6061 Al deposits, compared to conventionally processed 6061-T6 material. The increase in UTS was attributed to grain refinement and strain hardening mechanisms, while the decrease in ductility is the result of cold working experienced during CS as well as the presence of some interparticle voids and porosity. Post-deposition heat treatment led to an increase in the UTS and ductility in all conditions because of the formation of strengthening precipitates and the localized improvement in metallurgical bonding at the PPBs. Finally, the adhesion strength of the CS layer was evaluated by tensile pull-off and three lug shear testing methods with average adhesion strength of 78.2 and 88.5 MPa, respectively.

Acknowledgements

This work was performed under subcontract to the Pueblo Economic Development Corporation (PEDCO) under Army Research Lab contract no. W911NF-11-2-0014. The authors would like to thank Mike Carter et al. for coordinating the deposition of the material for this analysis. The authors also thank Dr. D. Butt and Dr. B. Jaques from Boise State University for help in performing microtensile testing of cold spray specimens. Dr. S.P. Ahrenkiel is gratefully acknowledged for his assistance with electron microscopy.

References

[1] J. Villafuerte, Modern Cold Spray: Materials, Process, and Applications, Springer, Berlin, 2015.
[2] T. Schmidt, F. Gärtner, H. Assadi, H. Kreye, Development of a generalized parameter window for cold spray deposition, Acta Mater. 54 (2006) 729–742.
[3] V.K. Champagne, The Cold Spray Materials Deposition Process: Fundamentals and Applications, Woodhead Publishing Limited, Cambridge, 2007.
[4] A.P. Alkhimov, V.F. Kosarev, A.N. Papyrin, A method of "cold" gas-dynamic deposition, Sov. Phys. Dokl. 35 (1990) 1047–1049.
[5] M.R. Rokni, C.A. Widener, G.A. Crawford, M.K. West, An investigation into microstructure and mechanical properties of cold sprayed 7075 Al deposition, Mater. Sci. Eng. A 625 (2015) 19–27.
[6] P. Vo, E. Irissou, J.G. Legoux, S. Yue, Mechanical and microstructural characterization of cold-sprayed Ti-6Al-4V after heat treatment, J. Therm. Spray Technol. 22 (2013) 954–964.
[7] M.R. Rokni, C.A. Widener, V.K. Champagne, G.A. Crawford, Microstructure and mechanical properties of cold sprayed 7075 deposition during non-isothermal annealing, Surf. Coat. Technol. 276 (2015) 305–315.
[8] V.K. Champagne III, M.K. West, M.R. Rokni, T. Curtis, V.R. Champagne Jr., B. McNally, Joining of cast ZE41A Mg to wrought 6061 Al by the cold spray process and friction stir welding, J. Therm. Spray Technol. 25 (2016) 143–159.
[9] P.D. Eason, J.A. Fewkes, S.C. Kennett, T.J. Eden, K. Tello, M.J. Kaufman, M. Tiryakioğlu, On the characterization of bulk copper produced by cold gas dynamic spray processing in as fabricated and annealed conditions, Mater. Sci. Eng. A 528 (2011) 8174–8178.
[10] H.J. Kim, C.-H. Lee, S.-Y. Hwang, Fabrication of WC–Co coatings by cold spray deposition, Surf. Coat. Technol. 191 (2005) 335–340.
[11] K. Spencer, M.-X. Zhang, Heat treatment of cold spray coatings to form protective intermetallic layers, Scr. Mater. 61 (2009) 44–47.
[12] Y. Zou, D. Goldbaum, J.A. Szpunar, S. Yue, Microstructure and nanohardness of cold-sprayed coatings: electron backscattered diffraction and nanoindentation studies, Scr. Mater. 62 (2010) 395–398.
[13] M.R. Rokni, C.A. Widener, A.T. Nardi, V.K. Champagne, Nano crystalline high energy milled 5083 Al powder deposited using cold spray, Appl. Surf. Sci. 305 (2014) 797–804.
[14] M.R. Rokni, C.A. Widener, G.A. Crawford, Surf. Coat. Technol. 251 (2014) 254–263.
[15] T. Schmidt, H. Assadi, F. Gärtner, H. Richter, T. Stoltenhoff, H. Kreye, T. Klassen, From particle acceleration to impact and bonding in cold spraying, J. Therm. Spray Technol. 18 (2009) 794–808.
[16] M.R. Rokni, C.A. Widener, S.P. Ahrenkiel, B.K. Jasthi, V.K. Champagne, Annealing behaviour of 6061 aluminium deposited by high pressure cold spray, Surf. Eng. 30 (2014) 361–368.
[17] M.R. Rokni, C.A. Widener, V.K. Champagne, Microstructural evolution of 6061 aluminum gas-atomized powder and high-pressure cold-sprayed deposition, J. Therm. Spray Technol. 23 (2014) 514–524.
[18] L. Ajdelsztajn, B. Jodoin, G.E. Kim, J.M. Schoenung, Cold spray deposition of nanocrystalline aluminum alloys, Metall. Mater. Trans. A 6 (2005) 657–666.
[19] D. Goldbaum, R.R. Chromik, S. Yue, E. Irissou, J.-G. Legoux, Mechanical property mapping of cold sprayed Ti splats and coatings, J. Therm. Spray Technol. 20 (2011) 486–496.
[20] F. Gärtner, T. Stoltenhoff, J. Voyer, H. Kreye, S. Riekehr, M. Koçak, Mechanical properties of cold-sprayed and thermally sprayed copper coatings, Surf. Coat. Technol. (2006) 6770–6782.
[21] X.-M. Meng, J.-B. Zhang, W. Han, J. Zhao, Y.-L. Liang, Influence of annealing treatment on the microstructure and mechanical performance of cold sprayed 304 stainless steel coating, Appl. Surf. Sci. 258 (2011) 700–704.
[22] B. AL-Mangour, P. Vo, R. Mongrain, E. Irissou, S. Yue, Effect of heat treatment on the microstructure and mechanical properties of stainless steel 316L coatings produced by cold spray for biomedical applications, J. Therm. Spray Technol. 23 (2014) 641–652.
[23] W.J. Kim, J.Y. Wang, Microstructure of the post-ECAP aging processed 6061 Al alloys, Mater. Sci. Eng. A 464 (2007) 23–27.
[24] M.R. Rezaei, M.R. Toroghinejad, F. Ashrafizadeh, Effects of ARB and ageing processes on mechanical properties and microstructure of 6061 aluminum alloy, J. Mater. Process. Technol. 211 (2011) 1184–1190.
[25] W.J. Kim, J.K. Kim, T.Y. Park, S.I. Hong, D.I. Kim, Y.S. Kim, J.D. Lee, Enhancement of strength and superplasticity in a 6061 Al alloy processed by equal-channel-angular-pressing, Metall. Mater. Trans. A 33 (2002) 3155–3164.
[26] G. Nurislamova, X. Sauvage, M. Murashkin, R. Islamgaliev, R. Valiev, Nanostructure and related mechanical properties of an Al–Mg–Si alloy processed by severe plastic deformation, Philos. Mag. Lett. 88 (2008) 459–466.
[27] R. Jayaganthan, Effects of warm rolling and ageing after cryogenic rolling on mechanical properties and microstructure of Al 6061 alloy, Mater. Des. 39 (2012) 226–233.
[28] M.H. Farshidi, M. Kazeminezhad, H. Miyamoto, Severe plastic deformation of 6061 aluminum alloy tube with pre and post heat treatments, Mater. Sci. Eng. A 563 (2013) 60–67.
[29] T. Suhonen, T. Varis, S. Dosta, M. Torrell, J.M. Guilemany, Residual stress development in cold sprayed al, cu and ti coatings, Acta Mater. 61 (2013) 6329–6337.
[30] R. Ghelichi, S. Bagherifard, D. MacDonald, I. Fernandez-Pariente, B. Jodoin, M. Guagliano, Experimental and numerical study of residual stress evolution in cold spray coating, Appl. Surf. Sci. 288 (2014) 26–33.
[31] R. Ghelichi, D. MacDonald, S. Bagherifard, H. Jahed, M. Guagliano, B. Jodoin, Microstructure and fatigue behavior of cold spray coated Al5052, Acta Mater. 60 (2012) 6555–6561.
[32] M.R. Rokni, C.A. Widener, V.K. Champagne, Microstructural stability of ultrafine grained cold sprayed 6061 aluminum alloy, Appl. Surf. Sci. 290 (2014) 482–489.
[33] ASM Committee on Gas Carburizing, Carbonitriding, and Nitriding, Gas Nitriding, Heat treatment, ASM Handbook, 4, American Society of Metals, Materials Park, OH 1991, p. 191.
[34] W.C. Oliver, G.M. Pharr, An improved technique for determining hardness and elastic modulus using load and displacement sensing indentation experiments, J. Mater. Res. 7 (1992) 1564.
[35] V.K. Champagne, The repair of magnesium rotorcraft components by cold spray, J. Fail. Anal. Prev. 8 (2008) 164–175.
[36] Y. Zou, W. Qin, E. Irissou, J.-G. Legoux, S. Yue, A.J. Szpunar, Dynamic recrystallization in the particle/particle interfacial region of cold-sprayed nickel coating: electron backscatter diffraction characterization, Scr. Mater. 61 (2009) 899–902.
[37] C. Borchers, F. Gärtner, T. Stoltenhoff, H. Kreye, Formation of persistent dislocation loops by ultra-high strain-rate deformation during cold spraying, Acta Mater. 53 (2005) 2991–3000.
[38] K.H. Kim, M. Watanabe, J. Kawakita, S. Kuroda, Grain refinement in a single titanium powder particle impacted at high velocity, Scr. Mater. 59 (2008) 768–771.
[39] O. Meydanoglu, J. Bertrand, E. Sabri Kayali, Microstructure, mechanical properties and corrosion performance of 7075 Al matrix ceramic particle reinforced composite coatings produced by the cold gas dynamic spraying process, Surf. Coat. Technol. 235 (2013) 108–116.
[40] M. Yandouzi, L. Ajdelsztajn, B. Jodoin, WC-based composite coatings prepared by the pulsed gas dynamic spraying process: effect of the feedstock powders, Surf. Coat. Technol. 202 (2008) 3866–3877.
[41] C.J. Li, W.Y. Li, Deposition characteristics of titanium coating in cold spraying, Surf. Coat. Technol. 167 (2003) 278–283.
[42] K. Ma, H. Wen, T. Hu, T.D. Topping, D. Isheim, D.N. Seidman, E.J. Lavernia, J.M. Schoenung, Mechanical behavior and strengthening mechanisms in ultrafine grain precipitation-strengthened aluminum alloy, Acta Mater. 62 (2014) 141–155.
[43] J.K. Jim, H.G. Jeong, S.I. Hong, Y.S. Kim, W.J. Kim, Effect of aging treatment on heavily deformed microstructure of a 6061 aluminum alloy after equal channel angular pressing, Scr. Mater. 45 (2001) 901–907.
[44] S.H. Lee, Y. Saito, T. Sakai, H. Utsunomiya, Microstructures and mechanical properties of 6061 aluminum alloy processed by accumulative roll-bonding, Mater. Sci. Eng. A 325 (2002) 228–235.
[45] W.Y. Li, C. Zhang, H. Liao, C. Coddet, Effect of heat treatment on microstructure and mechanical properties of cold sprayed Ti coatings with relatively large powder particles, J. Coat. Technol. Res. 6 (2009) 401–406.
[46] P. Sudharshan Phani, D. Srinivasa Rao, S.V. Joshi, G. Sundararajan, Effect of process parameters and heat treatments on properties of cold sprayed copper coatings, J. Therm. Spray Technol. 16 (2007) 425–434.
[47] W.Y. Li, C. Yang, H. Liao, Effect of vacuum heat treatment on microstructure and microhardness of cold-sprayed TiN particle-reinforced Al alloy-based composites, Mater. Des. 32 (2011) 388–394.

[48] Q. Wang, N. Birbilis, M.-X. Zhang, On the formation of a diffusion bond from cold-spray coatings, Metall. Mater. Trans A 43 (2012) 1395–1399.
[49] E. Irissou, J.G. Legoux, B. Arsenault, C. Moreau, J. Therm. Spray Technol. 16 (2007) 661–668.
[50] J. Wu, J. Yang, H. Fang, S. Yoon, C. Lee, Investigation of Al-Al2O3 cold spray coating formation and properties, Appl. Surf. Sci. 252 (2006) 7809–7814.
[51] D. Zhang, P.H. Shipway, D.G. McCartney, Cold gas dynamic spraying of aluminum: the role of substrate characteristics in deposit formation, J. Therm. Spray Technol. 14 (2005) 109–116.
[52] S. Shin, Y. Xiong, Y. Ji, H.J. Kim, C. Lee, The influence of process parameters on deposition characteristics of a soft/hard composite coating in kinetic spray process, Appl. Surf. Sci. 254 (2008) 2269–2275.